Diagnostic Power of Lamina Cribrosa Depth and Curvature in Glaucoma

Seung Hyen Lee,[1] Tae-Woo Kim,[1] Eun Ji Lee,[1] Michaël J. A. Girard,[2,3] and Jean Martial Mari[4]

[1]Department of Ophthalmology, Seoul National University College of Medicine, Seoul National University Bundang Hospital, Seongnam, Korea
[2]Department of Biomedical Engineering, National University of Singapore, Singapore
[3]Singapore Eye Research Institute, Singapore National Eye Centre, Singapore
[4]Université de la Polynésie française, Tahiti, French Polynesia

Correspondence: Tae-Woo Kim, Department of Ophthalmology, Seoul National University College of Medicine, Seoul National University Bundang Hospital, 300 Gumi-dong, Bundang-gu, Seongnam, Gyeonggi-do 13620, Korea; twkim7@snu.ac.kr.

Submitted: September 21, 2016
Accepted: December 22, 2016

Citation: Lee SH, Kim T-W, Lee EJ, Girard MJA, Mari JM. Diagnostic power of lamina cribrosa depth and curvature in glaucoma. *Invest Ophthalmol Vis Sci*. 2017;58:755–762. DOI:10.1167/iovs.16-20802

Purpose. To compare the capability of the lamina cribrosa depth (LCD) and lamina cribrosa (LC) curvature in discriminating between eyes with primary open-angle glaucoma (POAG) and healthy eyes.

Methods. Seventy-seven eyes of 77 patients with POAG and 77 eyes of 77 healthy subjects who were matched for age, sex, and axial length were included. The LCD and lamina cribrosa curvature index (LCCI) were measured in B-scan images obtained using swept-source optical coherence tomography at seven locations spaced equidistantly across the vertical optic disc diameter. The mean values of the measurements made at seven points of the LC were defined as the average LCD and LCCI.

Results. The average LCD (527.0 ± 116.4 vs. 413.3 ± 80.4 μm, $P < 0.001$) and average LCCI (10.97 ± 2.59 vs. 6.81 ± 1.43, $P < 0.001$) were significantly larger in POAG eyes than in the matched healthy subjects (all seven locations, $P < 0.001$). The area under the receiver operating characteristic curve (AUC) was significantly larger for the LCCI than the LCD (0.921 vs. 0.784, $P < 0.001$). The intraocular pressure was positively associated with average LCD and LCCI in healthy subjects ($P = 0.021$ and $P < 0.001$, respectively) and POAG patients ($P = 0.011$ and $P < 0.001$, respectively). Male sex was associated with larger average LCCI ($P = 0.013$) and LCD ($P = 0.008$) in POAG.

Conclusions. The LCCI had significantly better discriminating capability between POAG and healthy eyes than LCD. This finding suggests that the LCCI may serve better than the LCD for improved glaucoma management.

Keywords: lamina cribrosa, curvature, depth, glaucoma

The glaucomas are a group of disorders that are characterized by the loss of retinal ganglion cells and their axons and corresponding visual field defects. According to the mechanical theory of glaucoma, posterior deformation of the lamina cribrosa (LC) is a principal pathogenic event.[1] This hypothesis is supported by experimental studies demonstrating that deformation of the optic nerve head (ONH) structure preceded early surface structural damage[2,3] and early loss of the retinal nerve fiber layer (RNFL).[4] A clinical study also found that ONH surface depression occurs before RNFL thinning in a significant proportion of glaucoma patients.[5] The posterior deformation and associated compression of the LC are considered to cause axonal and/or retinal ganglion cell damage through diverse mechanisms including blockade of axonal transport and tissue remodeling by reactive astrocytes.[6–9] Furthermore, the compression of the LC may affect the diffusion of nutrients from the capillaries within the laminar beams to the adjacent axons, thereby further compromising the axons.[10]

Given the principal role of posterior LC bowing in glaucoma and given that the posterior LC deformation is not involved in other optic neuropathies,[11,12] a parameter that can describe LC morphology (and changes in morphology) might be potentially useful as an additional aid in making differential diagnoses from other optic neuropathies. In addition, it would be of interest to correlate the shape of the LC with the disease manifestation and progression. Such an investigation would enhance our insight into the role of the LC morphology in the development and progression of glaucomatous optic neuropathy, and might facilitate the development of tailored treatment strategies in patients with differing LC morphologies. For instance, early application of aggressive treatment may be applied in eyes with LC morphology that could be indicative of large LC deformation if such eyes are proven to be associated with fast progression. In contrast, non-IOP–lowering treatment or a conservative approach can be tried in patients with LC morphology indicating small LC deformation. The development of a morphologic index for the LC would therefore be meaningful from both the research and clinical perspectives.

A potential indicator of the LC morphology is the LC depth (LCD), since LCD is correlated with the magnitude of the posterior LC deformation. Studies have demonstrated that the LCD measured from the level of Bruch's membrane opening (BMO) is larger in eyes with primary open-angle glaucoma (POAG) than in healthy eyes.[13] In addition, a larger LCD has been demonstrated to be related to faster glaucoma progression.[14] However, measuring the LCD using the BMO level as the

reference plane would include the choroidal thickness. Since the LC is a sieve-like perforation in the posterior part of the sclera, which is sustained by load-bearing connective tissues of the peripapillary sclera, the choroid is not relevant to the LC deformation. Thus, including the choroidal thickness in the LCD would lead to a biased assessment of LC morphology. For instance, an eye with a thicker choroid would have a larger LCD than an eye with thinner choroid even when both eyes have the same posterior LC deformation. This limitation can be resolved by measuring the LCD from the level of the anterior scleral canal opening (ASCO) because this would not include the choroidal thickness. However, detection of ASCO is not established using the current imaging technologies.

Another indicator of the LC morphology is the LC curvature, since the LC deformation manifests as posterior bowing in response to elevation of the intraocular pressure (IOP).[2,15,16] The LC curvature is robust in that it is not affected by the choroidal thickness.

Considering that ONH excavation is the hallmark of glaucomatous optic neuropathy, we hypothesized that a parameter that represents the shape of the ONH connective tissue (i.e., the LC) could have ability to discriminate glaucomatous eyes from healthy eyes. The purpose of the present study was to compare the capability of the LC curvature and LCD in discriminating glaucomatous eyes from healthy eyes.

Methods

This investigation was based on ongoing prospective investigations of glaucoma patients at the Seoul National University Bundang Hospital Glaucoma Clinic: the Lamina Cribrosa Exploration Study (LCES)[17,18] and the Investigating Glaucoma Progression Study (IGPS).[19,20] Both studies recruited consecutive subjects who met the eligibility criteria and provided written informed consent to participate. This study was approved by the Seoul National University Bundang Hospital Institutional Review Board and followed the tenets of the Declaration of Helsinki.

Study Subjects

Each subject enrolled in the LCES and IGPS received comprehensive ophthalmic examinations that included visual acuity measurement, Goldmann applanation tonometry, refraction tests, slit-lamp biomicroscopy, gonioscopy, dilated stereoscopic examination of the optic disc, stereo disc photography (EOS D60 digital camera; Canon, Utsunomiya-shi, Tochigiken, Japan), swept-source optical coherence tomography (SS-OCT; Topcon, Tokyo, Japan), measurements of the central corneal thickness (CCT; Orbscan II; Bausch & Lomb Surgical, Rochester, NY, USA), axial length (AXL; IOLMaster version 5; Carl Zeiss Meditec, Dublin, CA, USA), and standard automated perimetry (Humphrey Field Analyzer II 750, 24-2 Swedish interactive threshold algorithm; Carl Zeiss Meditec). Both the LCES and IGPS excluded subjects with a history of previous intraocular surgery other than cataract extraction and glaucoma surgery, intraocular disease (e.g., diabetic retinopathy, retinal vein occlusion, or optic neuropathies), or neurologic disease (e.g., pituitary tumor) that could cause visual field loss.

Primary open-angle glaucoma was defined as the presence of glaucomatous optic neuropathy (i.e., rim thinning, notching, or RNFL defect), an associated glaucomatous visual field defect, and an open iridocorneal angle. Glaucomatous visual field defect was defined as (1) being outside the normal limits on the glaucoma hemifield test; (2) at least three abnormal points, with a <5% probability of being normal, one point with $P < 1\%$ by pattern deviation; or (3) a pattern standard deviation of <5% as confirmed on two consecutive reliable tests (fixation loss rate of ≤20%, and false-positive and false-negative error rates of ≤25%).

The healthy subjects had an IOP of ≤21 mm Hg with no history of increased IOP, an absence of a glaucomatous disc appearance, no visible RNFL defect on red-free photography, and a normal visual field. Absence of a glaucomatous disc appearance was defined as an intact neuroretinal rim without peripapillary hemorrhages, notches, or localized pallor. A normal visual field was defined as the absence of glaucomatous visual field defects and neurologic field defects. Healthy subjects in the control group were matched with the glaucoma group in terms of age, sex, and AXL using a frequency-matching method.

Eyes included in either the POAG or control group were required to have a best-corrected visual acuity of at least 20/40, spherical refraction within −6.0 to +5.0 diopters (D), and cylinder correction within −3.0 to +3.0 D without a tilted appearance (defined as a tilt ratio between the longest and shortest diameters of the optic disc of >1.3)[21,22] or torsion of the optic disc (defined as a torsion angle—the deviation of the long axis of the optic disc from the vertical meridian—of >15°).[22,23] This was because the LC may be distorted as a result of nonglaucomatous factors.

Eyes were also excluded when a good-quality image could not be obtained due to media opacity or lack of patient cooperation. When both eyes of a subject were eligible, one eye was chosen randomly for inclusion in the data analysis.

The baseline IOP was defined as the mean of at least two measurements made within 2 weeks before initiating IOP-lowering treatment for the POAG group. The scan IOP was defined as the IOP at the time of obtaining SS-OCT images.

Swept-Source Optical Coherence Tomography

Swept-source OCT was performed using the deep-range imaging (DRI)-OCT1 system (Topcon), which uses a wavelength-sweeping laser centered at 1050 nm as a light source, with a repetition rate of 100,000 Hz, yielding an 8-μm axial resolution in the tissue. The longer wavelength of light compared with spectral-domain optical coherence tomography (SD-OCT) enables deeper posterior penetration,[24] which may be advantageous for visualizing the peripheral LC and its insertion site.[25,26] Swept-source OCT scans were obtained using a 6-mm, 11 horizontal line raster scan protocol. The 1st and the 11th B-scans of the vertically equivalent 11 raster scans were positioned at the upper and lower margins of the optic disc, respectively. For each line scan, 32 single images were registered and averaged. Adjustment was made for the magnification error by entering the AXL before acquiring images.

To enhance the visibility of the peripheral LC, all images were postprocessed using adaptive compensation,[27,28] and the measurement was performed using the manual caliper tool of the DRI-OCT viewer (version 9.14) by glaucoma specialists (SHL and EJL) who were blinded to clinical information. The average LCD and lamina cribrosa curvature index (LCCI) were determined as the mean values of the measurements made at seven points of the LC. The mean of the measurements from each of the two observers was used in the analysis.

Measurement of LCD

Among 11 B-scans of each eye, two scans each at superior and inferior periphery were excluded from the measurement because it was often difficult to see the anterior LC surface in this region. Therefore, the LCD was measured at the seven

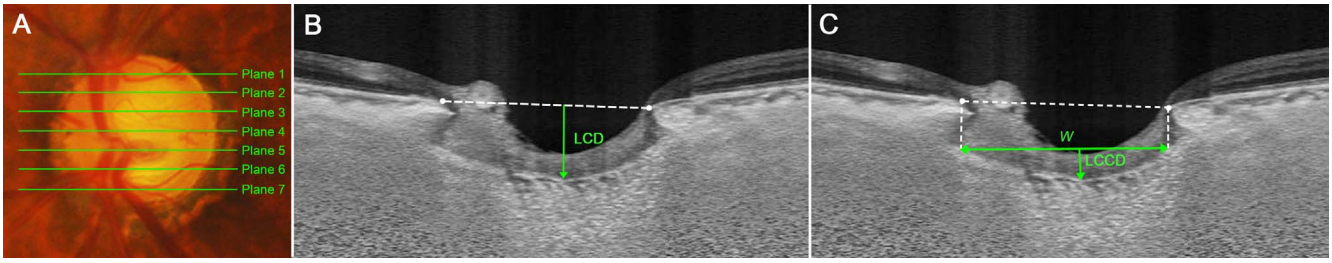

Figure 1. Measurement of the lamina cribrosa depth (LCD) and lamina cribrosa curvature index (LCCI). (**A**) Disc photograph showing seven horizontal *green lines* that indicate the locations at which the measurements were performed. (**B**, **C**) Swept-source optical coherence tomography (SS-OCT) B-scan images obtained in plane 4 as shown in (**A**). (**B**) The LCD was measured as the distance from the reference line connecting the two Bruch's membrane opening (BMO) points to the anterior surface of the lamina cribrosa (LC). The LCD was measured at the maximally depressed point. (**C**) The LCCI was measured by dividing the lamina cribrosa curve depth (LCCD) by the width of the anterior LC surface reference line (*W*) and multiplying by 100.

locations equidistant across the vertical optic disc diameter using horizontal SS-OCT B-scan images. These seven B-scan lines were defined as plane 1 to plane 7 (superior to inferior regions, Fig. 1). In this model, plane 4 corresponds to the midhorizontal plane, and planes 2 and 6 correspond approximately to the superior and inferior midperiphery, respectively. To determine the LCD, a line connecting the edges of BMO was set as a reference plane (BMO reference line), and then the LCD was measured in the direction perpendicular to the reference plane at the maximally depressed point (Fig. 1).

Measurement of LCCI

To quantify the posterior bowing of the LC on the SS-OCT B-scan images, we defined the LCCI as the inflection of a curve representing a section of the LC. To measure the LCCI, a new reference line (LC surface reference line) was set in each B-scan by connecting the two points on the anterior LC surface that met with the lines drawn from each Bruch's membrane termination point perpendicularly to the BMO reference line. The length of this reference line was defined as width (*W*). Then, the lamina cribrosa curve depth (LCCD) was determined as the maximum depth from this reference line to the anterior LC surface (Fig. 1). The LCCI was then calculated as (LCCD/*W*) $\times$ 100. Since the curvature was thereby normalized according to the LC width, it describes the shape of the LC independent of the actual size of the ONH. Only the LC within BMO was considered because the LC was often not clearly visible outside of BMO. In eyes with LC defects, the LCD and LCCI were measured using a presumed anterior LC surface that best fit the curvature of the remaining part of the LC or excluding the area of LC defect.

Statistical Analysis

The Bland-Altman limits of agreement were used to measure the interobserver reproducibility of measurements of the LCD and LCCI. Differences in continuous variables between two groups were compared using independent *t*-tests, while categorical variables were compared using χ^2 test. Between-group differences in the LCD and LCCI were evaluated using paired *t*-tests, and raw data were subjected to Bonferroni correction on the basis of the number of comparisons in each analysis. The area under the receiver operating characteristic curve (AUC) was calculated to assess the ability of each testing parameter in differentiating glaucoma from healthy eyes, where AUCs of 1.0 and 0.5 represent perfect and chance discrimination, respectively.[29] In addition, linear regression analyses were performed to assess the associations between various clinical factors and LC parameters. All statistical analyses were performed using Statistical Package for Social Sciences software (version 22.0 for Windows; SPSS, Chicago, IL, USA). MedCalc (version 16.4.3, Ostend, Belgium; www.medcalc.be) was used for comparing AUC between the LCD and LCCI. Except where indicated otherwise, the data are presented as mean $\pm$ SD values, and the cutoff for statistical significance was set at $P < 0.05$.

Results

This cross-sectional study initially involved 150 POAG patients and 127 healthy subjects, among whom 41 POAG patients and 23 healthy subjects were excluded due to the presence of a tilted disc. A further nine subjects were excluded due to poor image quality preventing the clear visualization of the anterior LC surface in at least two of the seven SS-OCT B-scan disc images. After matching for age, sex, and AXL between groups, 77 eyes of 77 POAG patients and 77 eyes of 77 healthy subjects were finally included.

Table 1 summarizes the clinical demographics of the included subjects. There were no significant differences in age, sex, spherical equivalent, scan IOP, CCT, or AXL between POAG patients and healthy subjects. However, significant differences were found between the two groups for the mean deviation and pattern standard deviation of the visual field tests and the global RNFL thickness (all $P < 0.001$).

The 95% Bland-Altman limits of agreement between the measurements from the two glaucoma specialists were −21.17 to 27.51 μm for the LCD and −1.53 to 1.47 for the LCCI (Fig. 2).

Table 1. Demographic Characteristics of the Study Subjects

Characteristics	Healthy, $n = 77$	POAG, $n = 77$	*P* Value
Age, y	62.6 ± 10.9	62.4 ± 11.0	0.883
Female (%)	54 (70.1)	54 (70.1)	1.000
SE, D	0.04 ± 2.03	−0.25 ± 2.04	0.387
AXL, mm	23.61 ± 0.96	23.64 ± 0.98	0.871
CCT, μm	557.1 ± 35.8	542.9 ± 77.2	0.167
Baseline IOP, mm Hg	n/a	17.3 ± 5.5	
Scan IOP, mm Hg	12.9 ± 2.8	14.0 ± 5.5	0.123
VF MD, dB	−0.86 ± 1.55	−10.44 ± 7.01	**<0.001**
VF PSD	1.89 ± 0.83	9.09 ± 3.76	**<0.001**
Global RNFL thickness, μm	69.9 ± 13.8	102.5 ± 7.2	**<0.001**

Data are mean ± standard deviation or *n* (%) values, with statistically significant *P* values in boldface. SE, spherical equivalent; D, diopter; AXL, axial length; CCT, central corneal thickness; IOP, intraocular pressure; VF, visual field; MD, mean deviation; dB, decibel; PSD, pattern standard deviation; RNFL, retinal nerve fiber layer; n/a, not applicable.

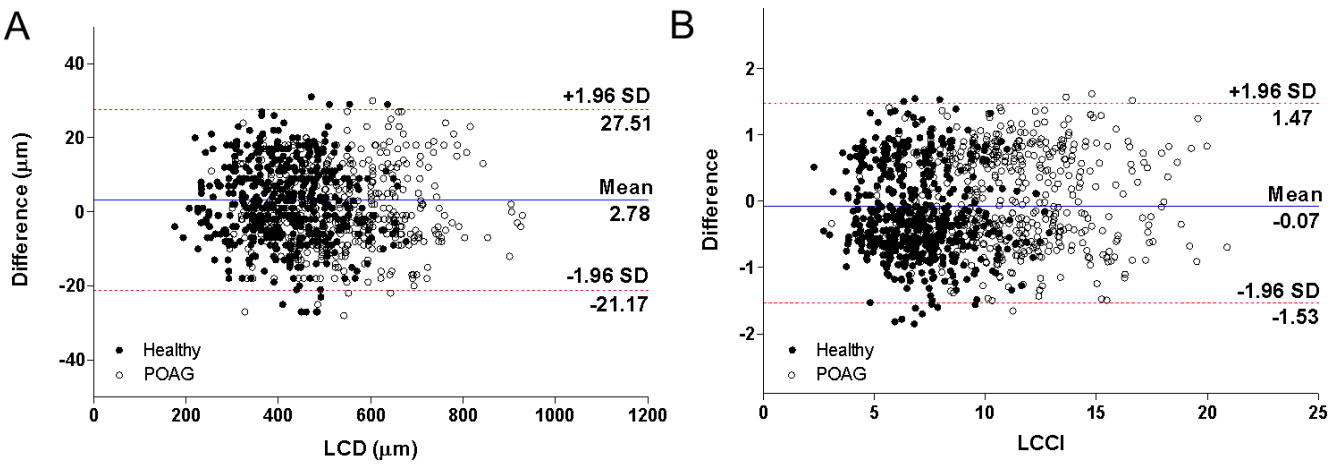

FIGURE 2. Bland-Altman plots showing the interobserver reproducibility in measuring the LCD and LCCI. The *solid line* represents the mean difference ([**A**] 2.78 ± 10.7 μm; [**B**] −0.07 ± 0.70) and the two *dotted lines* represent the 95% limits of agreement.

Comparison of LCD and LCCI

Table 2 compares the LCD and LCCI between POAG and healthy eyes. The LCD and LCCI were significantly larger in POAG eyes than in healthy eyes at all seven measured planes (all $P < 0.001$; Table 2; Fig. 3). The LCD was larger in the superior midperiphery than the inferior midperiphery. The LCCI had similar increased values in both superior and inferior regions at distances farther from the midhorizontal plane, where the LCCI was the least.

Figure 4 shows the distribution of the LCD and LCCI in both groups. The upper 95th percentile values of the average LCD and LCCI in healthy subjects were 538.44 μm and 9.51, respectively. The LCD and the LCCI were larger than the upper 95th percentile values in healthy subjects in 18 (23.4%) and 48 (62.3%) POAG patients, respectively.

Figure 5 shows the comparison of the AUC values between the LCD and LCCI to discrimitate between POAG and healthy subjects. The AUC was significantly larger for the LCCI than the LCD (0.921 vs. 0.784, $P < 0.001$). The diagnostic values of LCD, LCCI, and global RNFL thickness were compared using receiver operating characteristic curve anaylsis (Table 3). Among the measurements of parameters, global RNFL thickness had the largest AUC (0.985; 95% confidence interval [CI], 0.938–0.999) for discriminating glaucoma patients from healthy subjects.

Factors Influencing LCD and LCCI

In healthy eyes, younger age and higher scan IOP were associated with a larger average LCCI in the univariate analysis. In the multivariate analysis, only a higher scan IOP was significantly associated with a larger LCCI. Only higher scan IOP was associated with a larger LCD in both univariate and multivariate analyses (Table 4). In the POAG group, higher scan IOP, higher baseline IOP, and male sex were significantly associated with both larger LCD and LCCI in the univariate analysis, with higher scan IOP and male sex remaining as significant factors in the multivariate analysis. Younger age was associated with greater LCD in the univariate analysis, but it was marginally significant in the multivariate analysis (Table 4).

Representative Cases

A pair of representative cases showing the discrepancy between LCD and LCCI is presented in Figure 6. While the LCD was larger in the shown healthy eye than the POAG eye, the LCCI was larger in the POAG eye.

DISCUSSION

In comparing two candidate indicators of the LC morphology (i.e., LCD and LCCI), the present study has demonstrated that the efficacy in discriminating between POAG and healthy eyes was better for the LCCI than the LCD. To the best of our knowledge, this is the first study to compare the LCD and curvature simultaneously in POAG and healthy eyes.

Lamina cribrosa depth has been utilized in both experimental and clinical studies after the emergence of SD-OCT.[14,30,31] Until now, the LCD has been measured from

TABLE 2. Comparison of Lamina Cribrosa Curvature Index (LCCI) and Lamina Cribrosa Depth (LCD) Between Healthy and POAG Eyes

	LCCI			LCD, μm		
Plane Number	**Healthy, $n = 77$**	**POAG, $n = 77$**	***P* Value**	**Healthy, $n = 77$**	**POAG, $n = 77$**	***P* Value**
1	7.36 ± 1.57	11.42 ± 3.01	**<0.001**	434.1 ± 93.7	553.1 ± 127.9	**<0.001**
2	7.26 ± 1.77	11.03 ± 3.15	**<0.001**	439.6 ± 91.0	558.4 ± 131.5	**<0.001**
3	6.78 ± 1.88	10.48 ± 3.03	**<0.001**	433.9 ± 95.1	542.9 ± 129.0	**<0.001**
4	6.24 ± 1.84	10.22 ± 2.96	**<0.001**	412.2 ± 91.4	520.4 ± 118.2	**<0.001**
5	6.43 ± 1.70	10.72 ± 3.02	**<0.001**	403.9 ± 91.3	511.7 ± 114.9	**<0.001**
6	6.51 ± 1.62	11.17 ± 3.30	**<0.001**	389.2 ± 80.3	509.2 ± 116.6	**<0.001**
7	6.98 ± 1.84	11.60 ± 3.37	**<0.001**	379.7 ± 80.4	493.6 ± 115.8	**<0.001**
Average	6.81 ± 1.43	10.97 ± 2.59	**<0.001**	413.3 ± 80.4	527.0 ± 116.4	**<0.001**

Data are mean ± standard deviation values, with statistically significant *P* values in boldface. Bonferroni correction was applied to raw data for measurements in the seven locations. Values that were significant after Bonferroni correction ($P < 0.007$; 0.05/7) are shown in bold.

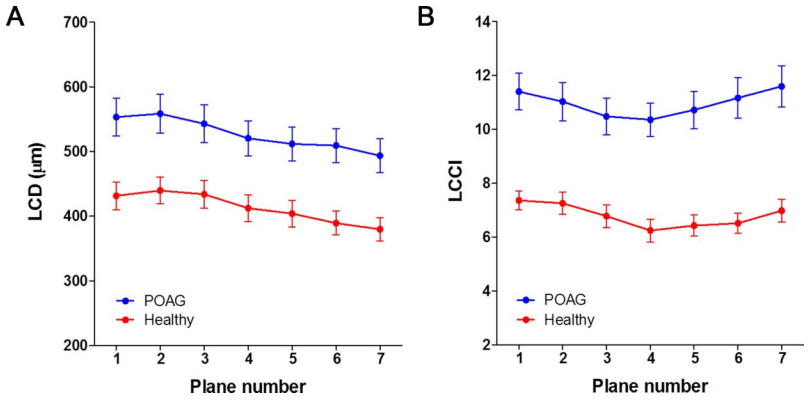

FIGURE 3. LCD (**A**) and LCCI (**B**) profiles in seven horizontal SS-OCT scans (planes 1 and 7 correspond to the superior- and inferior-most planes, respectively) in the healthy and primary open-angle glaucoma (POAG) groups. The mean LCD and LCCI were significantly larger in POAG than in healthy eyes in all seven scans (all $P < 0.001$). Note that the LCD is largest in the superior planes and gradually decreases when moving to the inferior region in both the POAG and healthy groups. In contrast, the LCCI increases similarly with distance from the midhorizontal plane.

BMO as the reference plane to the anterior surface of the LC,[22,24] which includes the choroidal thickness. However, the LC is a sieve-like perforation in the posterior part of the sclera and is sustained by load-bearing connective tissues of the peripapillary sclera. Thus, it would be more reasonable to assess LC morphology (and changes with IOP) from the scleral plane or directly within the LC. Measuring this value from the BMO level would inappropriately include the choroidal thickness, leading to a biased measurement. In contrast, the LCCI is not affected by the choroidal thickness, which can explain why the discriminating efficacy was better for the LCCI than the LCD.

The LCD was largest superiorly, which is consistent with the findings of previous studies.[13,32] In contrast, the LCCI did not differ between superior and inferior regions. We attribute this discrepancy to the choroidal thickness. It is known that the choroid is thicker superiorly than inferiorly,[33] and so the LCD would be larger in the superior region even though the LC is less bowed compared to the inferior region. This discrepancy highlights the limitation of using the LCD. It is known that glaucomatous damage occurs most often in the inferior region, followed by the superior region. The larger LCD in the superior region is not consistent with this preferential location of glaucomatous damage. In contrast, the larger LCCI both superiorly and inferiorly than in the midhorizontal plane is consistent with the preferential location of glaucomatous damage. Together these observations indicate that while the LC deforms in both superior and inferior regions as assessed using the LCCI, inferior deformation would be masked when it is evaluated using the LCD.

It is noteworthy that the LCCI was not zero in healthy eyes. The slight curvature may be due to a physiological feature of the posterior shell of the globe and/or the result of the translaminar pressure difference (TLPD). While the normal limits of IOP range from 10 to 21 mm Hg, that of the cerebrospinal fluid (CSF) pressure ranges from 5 to 15 mm Hg.[34,35] It is therefore possible that the TLPD is generally positive, resulting in posterior bowing of the LC. The curved nature of the LC in healthy eyes suggests that the optic nerve axons may have some resistance against slight bowing of the LC. In other words, axonal damage occurs when the LCCI exceeds a certain threshold, although the value may slightly vary among individuals. The 95% upper limit of the LCCI was 9.51; the threshold may be around this value, although it needs to be refined in a future larger study.

The AUC of LCCI (0.921) observed in the present study was comparable to previously reported respective values of other diagnostic parameters. Among various parameters, global peripapillary RNFL thickness and ONH rim area have been reported to have AUC ranging from 0.87 to 0.94[36–38] and 0.77 to 0.97,[39–41] respectively. The high AUC of the LCCI suggests that this parameter can be used as an aid to diagnose glaucoma. Considering that LC deformation may precede loss of the

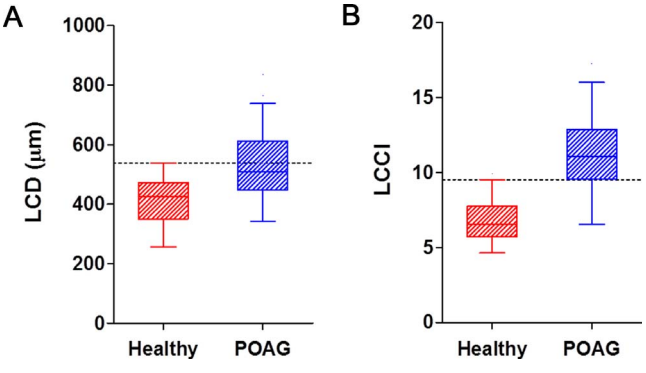

FIGURE 4. Box plots showing the distributions of the LCD (**A**) and LCCI (**B**) in healthy and POAG eyes. *Dashed lines* indicate the upper 95th percentile values in healthy subjects for the LCD and LCCI (538.44 μm and 9.51, respectively). This plot shows that overlap range between healthy and POAG eyes is larger for the LCD than the LCCI.

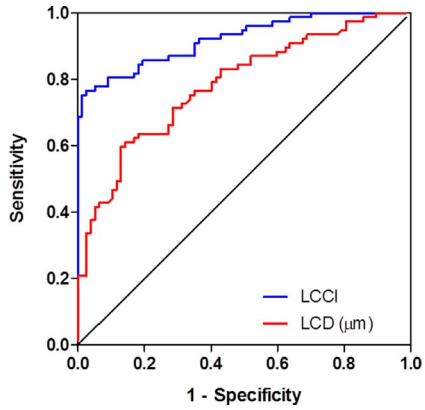

FIGURE 5. Receiver operating characteristic curves for the LCD and LCCI. The areas under these curves for the LCD and LCCI were 0.784 (95% confidence interval [CI], 0.712–0.855) and 0.921 (95% CI, 0.879–0.963), respectively.

Table 3. Diagnostic Power of the LCD, LCCI, and Global RNFL Thickness

	AUC	95% CI	Sensitivity at Specificity > 90%
LCD, μm	0.784	0.710–0.846	0.43
LCCI	0.921	0.866–0.958	0.81
Global RNFL thickness, μm	0.989	0.957–0.999	0.96

UC, area under the receiver operating characteristic curve; CI, confidence interval; LCD, lamina cribrosa depth; LCCI, lamina cribrosa curvature index; RNFL, retinal nerve fiber layer.

RNFL, this parameter may be particularly helpful in diagnosing early-stage glaucoma. In addition, this parameter may be useful when performing differential diagnoses from other optic neuropathies. Recent experimental and clinical studies have found that posterior LC deformation is not involved in nonglaucomatous optic nerve damage,[11,12] which suggests that the LCCI is useful for differentiating glaucoma from other optic neuropathies. It is noteworthy that many POAG patients were receiving IOP-lowering treatment at the time of SS-OCT scan. Previously, our group demonstrated that the posteriorly bowed LC in POAG patients may become less curved after IOP-lowering treatment. Based on this finding, it may be supposed that the POAG patients included in this study might have had greater LCCI before receiving IOP-lowering treatment than at the time of SS-OCT scan. Thus, if the LCCI were measured at the treatment-naïve status, it might have greater diagnostic power. Further study is warranted to evaluate the utility of the LCCI as a diagnostic tool.

It is intriguing that the LCCI was smaller than the upper 95th percentile value in healthy eyes in 37.3% of the POAG eyes. Two possibilities can be considered for these patients. First, the patients may have had low LCCI even at treatment-naïve status. Second, it is possible that the patients had high LCCI before receiving IOP-lowering treatment but their LCCI decreased to the current level after receiving IOP-lowering treatment; we have previously demonstrated the flattening of the LC after IOP-lowering treatment. Assuming that some of those eyes had a smaller LCCI even at treatment-naïve status, the finding may support the notion that factors other than translaminar strain play a relatively large role in some POAG patients. It would be interesting to determine whether other non-IOP–related factors such as vascular compromise (e.g., primary vascular dysregulation or low ocular perfusion pressure) or sleep apnea are more frequent in this population.

The present study used SS-OCT, which allows deeper penetration than SD-OCT due to the use of light with a longer wavelength.[24] This characteristic was helpful for delineating the anterior LC surface in healthy eyes with a thick neuroretinal rim. Furthermore, postprocessing using adaptive compensation further enhanced the delineation of the anterior LC surface. However, the anterior LC surface could still not be delineated in the scans farthest from the center of the optic disc in some eyes due to vascular shadowing and/or the thickness of the neuroretinal rim. For that reason, only the seven central-most scans were included in the analysis in the present study.

The findings of this study should be considered in the light of its limitations. First, a LC surface reference line should be set from the LC insertion points to allow the precise quantification of LC curvature. However, only the LC within the BMO width was included for measuring the LC curvature in the present study, since the LC was often not visible outside of this region. However, we previously demonstrated that the LCCI measured from the whole LC (between the LC insertions) was

Table 4. Factors Associated With the Average LCCI and LCD in Healthy and POAG Eyes ($n = 77$)

	LCCI								LCD							
	Healthy				POAG				Healthy				POAG			
	Univariate		Multivariate		Univariate		Multivariate		Univariate		Multivariate		Univariate		Multivariate	
Variables	Beta	*P* Value	Beta	*P* Value	Beta	*P* Value	Beta	*P* Value	Beta	*P* Value	Beta	*P* Value	Beta	*P* Value	Beta	*P* Value
Age, y	**−0.031**	**0.041**	−0.159	0.130	−0.020	0.461			−1.548	0.082	−0.161	0.155	**−3.290**	**0.006**	−0.248	0.057
Sex, female	−0.335	0.351			**−1.566**	**0.014**	**−1.478**	**0.013**	−20.132	0.340			**−95.971**	**0.001**	**−76.862**	**0.008**
SE, D	−0.158	0.081	−0.168	0.108	−0.110	0.467			−4.037	0.456			−12.485	0.064	1.630	0.842
AXL, mm	0.288	0.093	0.136	0.195	0.311	0.307			1.691	0.868			21.856	0.108		
CCT, μm	0.008	0.101			−0.001	0.738			0.215	0.451			−0.043	0.821		
Global RNFLT, μm	0.008	0.716			−0.036	0.091	0.001	0.978	1.601	0.238			−1.448	0.134		
Baseline IOP, mm Hg					0.173	**0.001**	0.059	0.422					**6.748**	**0.005**	1.719	0.619
Scan IOP, mm Hg	**0.233**	**<0.001**	**0.236**	**<0.001**	**0.183**	**0.001**	**0.178**	**<0.001**	**7.803**	**0.021**	**0.263**	**0.021**	**6.049**	**0.012**	**5.699**	**0.011**
MD, dB	−0.136	0.425			−0.067	0.140			−8.034	0.473			−2.912	0.149		
PSD, dB	−0.157	0.624			−0.025	0.771			−20.724	0.322			1.142	0.764		

Only variables with $P < 0.1$ on univariate analysis were included in the multivariate model. Values with statistical significance are in boldface. SE, spherical equivalent; D, diopter; AXL, axial length; CCT, central corneal thickness; RNFLT, retinal nerve fiber layer thickness; IOP, intraocular pressure; MD, mean deviation; dB, decibel; PSD, pattern standard deviation.

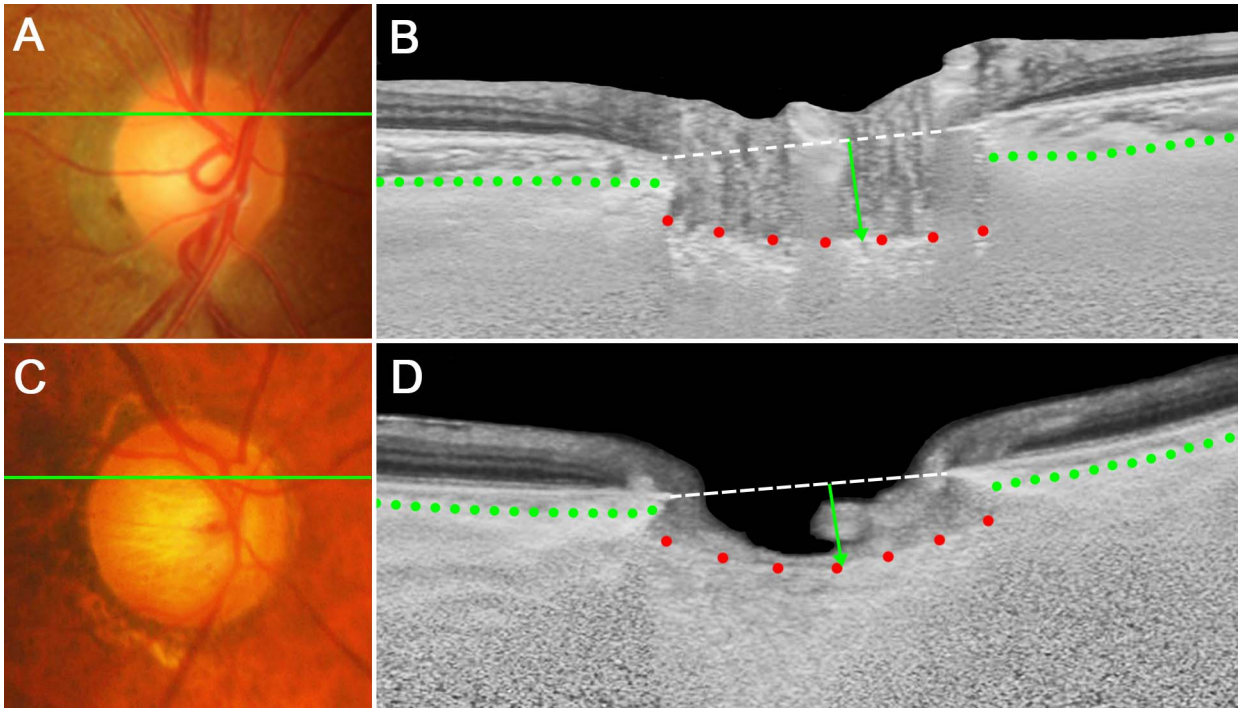

FIGURE 6. The LCD (*green arrows*) from BMO (*white dotted lines*) is larger in the healthy eye (**A**, **B**) while the LC is posteriorly curved (*red dots*) only in the glaucomatous eye (**C**, **D**). Note that the peripapillary choroid is much thicker in the healthy eye. The comparison of these two representative cases indicates that the LCD measured from BMO can misrepresent the LC morphology due to individual variations in the choroidal thickness.

comparable with that measured on the LC within BMO in eyes in which the LC was visible up to the LC insertion.[42] Thus, we consider that the curvature of the LC assessed within BMO may be used as a surrogate for the actual LC curvature. Meanwhile, due to this study design, the magnitude of posterior migration of the peripheral LC or the position of LC scleral insertion could not be considered. Further study regarding the relationship between the peripheral LC insertion and the LCCI is needed. Second, we referred to the change in the LC configuration as a change in curvature. However, a curvature is a geometric entity that refers specifically to the inverse of the radius of the arc of a circle that best fits the portion of a curve. Therefore, the LCCI does not correspond exactly to the actual LC curvature. Third, measurements were made manually rather than using an automated algorithm, which could have resulted in observer-related bias. In addition, inconvenience of manual calculation would be a barrier for application of LCCI in clinical practice. If automatic detection of the anterior LC surface and assessment of LC morphology become possible, it may facilitate the clinical use of LC morphology evaluation. Fourth, eyes with a tilted or torted optic disc were excluded, and so the reported findings cannot be directly applied to those eyes. Fifth, this study included only Korean patients, and so it is possible that the present findings cannot be extrapolated to other ethnic populations.

In conclusion, the efficacy in discriminating between glaucomatous and healthy eyes was better for the LCCI. This finding suggests that the LC curvature may be a better parameter than the LCD for evaluating the LC morphology.

Acknowledgments

Supported by Grant No. 02-2016-023 from the Seoul National University Bundang Hospital Research Fund. The funding organization played no role in the design or conduct of this research.

Disclosure: **S.H. Lee**, None; **T.-W. Kim**, Topcon (C); **E.J. Lee**, None; **M.J.A. Girard**, None; **J.M. Mari**, None

References

1. Quigley HA, Addicks EM, Green WR, Maumenee AE. Optic nerve damage in human glaucoma. II. The site of injury and susceptibility to damage. *Arch Ophthalmol*. 1981;99:635–649.
2. Bellezza AJ, Rintalan CJ, Thompson HW, Downs JC, Hart RT, Burgoyne CF. Deformation of the lamina cribrosa and anterior scleral canal wall in early experimental glaucoma. *Invest Ophthalmol Vis Sci*. 2003;44:623–637.
3. Yang H, Downs JC, Bellezza A, Thompson H, Burgoyne CF. 3-D histomorphometry of the normal and early glaucomatous monkey optic nerve head: prelaminar neural tissues and cupping. *Invest Ophthalmol Vis Sci*. 2007;48:5068–5084.
4. Strouthidis NG, Fortune B, Yang H, Sigal IA, Burgoyne CF. Longitudinal change detected by spectral domain optical coherence tomography in the optic nerve head and peripapillary retina in experimental glaucoma. *Invest Ophthalmol Vis Sci*. 2011;52:1206–1219.
5. Xu G, Weinreb RN, Leung CK. Optic nerve head deformation in glaucoma: the temporal relationship between optic nerve head surface depression and retinal nerve fiber layer thinning. *Ophthalmology*. 2014;121:2362–2370.
6. Anderson DR, Hendrickson A. Effect of intraocular pressure on rapid axoplasmic transport in monkey optic nerve. *Invest Ophthalmol*. 1974;13:771–783.
7. Minckler DS, Bunt AH, Johanson GW. Orthograde and retrograde axoplasmic transport during acute ocular hypertension in the monkey. *Invest Ophthalmol Vis Sci*. 1977;16:426–441.
8. Minckler DS, Tso MO. A light microscopic, autoradiographic study of axoplasmic transport in the normal rhesus optic nerve head. *Am J Ophthalmol*. 1976;82:1–15.

9. Hernandez MR. The optic nerve head in glaucoma: role of astrocytes in tissue remodeling. *Prog Retin Eye Res*. 2000;19:297–321.
10. Burgoyne CF, Downs JC, Bellezza AJ, Suh JK, Hart RT. The optic nerve head as a biomechanical structure: a new paradigm for understanding the role of IOP-related stress and strain in the pathophysiology of glaucomatous optic nerve head damage. *Prog Retin Eye Res*. 2005;24:39–73.
11. Ing E, Ivers KM, Yang H, et al. Cupping in the monkey optic nerve transection model consists of prelaminar tissue thinning in the absence of posterior laminar deformation. *Invest Ophthalmol Vis Sci*. 2016;57:2598–2611.
12. Lee EJ, Choi YJ, Kim TW, Hwang JM. Comparison of the deep optic nerve head structure between normal-tension glaucoma and nonarteritic anterior ischemic optic neuropathy. *PLoS One*. 2016;11:e0150242.
13. Park SC, Brumm J, Furlanetto RL, et al. Lamina cribrosa depth in different stages of glaucoma. *Invest Ophthalmol Vis Sci*. 2015;56:2059–2064.
14. Lee EJ, Kim TW, Kim M, Kim H. Influence of lamina cribrosa thickness and depth on the rate of progressive retinal nerve fiber layer thinning. *Ophthalmology*. 2015;122:721–729.
15. Yan DB, Coloma FM, Metheetrairut A, Trope GE, Heathcote JG, Ethier CR. Deformation of the lamina cribrosa by elevated intraocular pressure. *Br J Ophthalmol*. 1994;78:643–648.
16. Gaasterland D, Kupfer C. Experimental glaucoma in the rhesus monkey. *Invest Ophthalmol*. 1974;13:455–457.
17. Lee EJ, Kim TW, Weinreb RN. Improved reproducibility in measuring the laminar thickness on enhanced depth imaging SD-OCT images using maximum intensity projection. *Invest Ophthalmol Vis Sci*. 2012;53:7576–7582.
18. Lee EJ, Kim TW, Weinreb RN, Park KH, Kim SH, Kim DM. Visualization of the lamina cribrosa using enhanced depth imaging spectral-domain optical coherence tomography. *Am J Ophthalmol*. 2011;152:87–95, e81.
19. Kim YW, Lee EJ, Kim TW, Kim M, Kim H. Microstructure of beta-zone parapapillary atrophy and rate of retinal nerve fiber layer thinning in primary open-angle glaucoma. *Ophthalmology*. 2014;121:1341–1349.
20. Choi YJ, Lee EJ, Kim BH, Kim TW. Microstructure of the optic disc pit in open-angle glaucoma. *Ophthalmology*. 2014;121:2098–2106.
21. Jonas JB, Papastathopoulos KI. Optic disc shape in glaucoma. *Graefes Arch Clin Exp Ophthalmol*. 1996;234(suppl 1):S167–S173.
22. Vongphanit J, Mitchell P, Wang JJ. Population prevalence of tilted optic disks and the relationship of this sign to refractive error. *Am J Ophthalmol*. 2002;133:679–685.
23. Samarawickrama C, Mitchell P, Tong L, et al. Myopia-related optic disc and retinal changes in adolescent children from singapore. *Ophthalmology*. 2011;118:2050–2057.
24. Miki A, Ikuno Y, Jo Y, Nishida K. Comparison of enhanced depth imaging and high-penetration optical coherence tomography for imaging deep optic nerve head and parapapillary structures. *Clin Ophthalmol*. 2013;7:1995–2001.
25. Park HY, Shin HY, Park CK. Imaging the posterior segment of the eye using swept-source optical coherence tomography in myopic glaucoma eyes: comparison with enhanced-depth imaging. *Am J Ophthalmol*. 2014;157:550–557.
26. Takayama K, Hangai M, Kimura Y, et al. Three-dimensional imaging of lamina cribrosa defects in glaucoma using swept-source optical coherence tomography. *Invest Ophthalmol Vis Sci*. 2013;54:4798–4807.
27. Girard MJ, Strouthidis NG, Ethier CR, Mari JM. Shadow removal and contrast enhancement in optical coherence tomography images of the human optic nerve head. *Invest Ophthalmol Vis Sci*. 2011;52:7738–7748.
28. Mari JM, Strouthidis NG, Park SC, Girard MJ. Enhancement of lamina cribrosa visibility in optical coherence tomography images using adaptive compensation. *Invest Ophthalmol Vis Sci*. 2013;54:2238–2247.
29. Swets JA. Measuring the accuracy of diagnostic systems. *Science*. 1988;240:1285–1293.
30. Furlanetto RL, Park SC, Damle UJ, et al. Posterior displacement of the lamina cribrosa in glaucoma: in vivo interindividual and intereye comparisons. *Invest Ophthalmol Vis Sci*. 2013;54:4836–4842.
31. Yang H, He L, Gardiner SK, et al. Age-related differences in longitudinal structural change by spectral-domain optical coherence tomography in early experimental glaucoma. *Invest Ophthalmol Vis Sci*. 2014;55:6409–6420.
32. Seo JH, Kim TW, Weinreb RN. Lamina cribrosa depth in healthy eyes. *Invest Ophthalmol Vis Sci*. 2014;55:1241–1251.
33. Jiang R, Wang YX, Wei WB, Xu L, Jonas JB. Peripapillary choroidal thickness in adult Chinese: the Beijing Eye Study. *Invest Ophthalmol Vis Sci*. 2015;56:4045–4052.
34. Nathan BR. Cerebral correlates of hyponatremia. *Neurocrit Care*. 2007;6:72–78.
35. Berdahl JP, Allingham RR, Johnson DH. Cerebrospinal fluid pressure is decreased in primary open-angle glaucoma. *Ophthalmology*. 2008;115:763–768.
36. Leite MT, Rao HL, Zangwill LM, Weinreb RN, Medeiros FA. Comparison of the diagnostic accuracies of the Spectralis, Cirrus, and RTVue optical coherence tomography devices in glaucoma. *Ophthalmology*. 2011;118:1334–1339.
37. Leung CK, Chan WM, Yung WH, et al. Comparison of macular and peripapillary measurements for the detection of glaucoma: an optical coherence tomography study. *Ophthalmology*. 2005;112:391–400.
38. Park HY, Park CK. Diagnostic capability of lamina cribrosa thickness by enhanced depth imaging and factors affecting thickness in patients with glaucoma. *Ophthalmology*. 2013;120:745–752.
39. Wollstein G, Ishikawa H, Wang J, Beaton SA, Schuman JS. Comparison of three optical coherence tomography scanning areas for detection of glaucomatous damage. *Am J Ophthalmol*. 2005;139:39–43.
40. Rao HL, Zangwill LM, Weinreb RN, Sample PA, Alencar LM, Medeiros FA. Comparison of different spectral domain optical coherence tomography scanning areas for glaucoma diagnosis. *Ophthalmology*. 2010;117:1692–1699.e1.
41. Mwanza J-C, Durbin MK, Budenz DL, et al. Glaucoma diagnostic accuracy of ganglion cell–inner plexiform layer thickness: comparison with nerve fiber layer and optic nerve head. *Ophthalmology*. 2012;119:1151–1158.
42. Lee SH, Yu D-A, Kim T-W, Lee EJ, Girard MJA, Mari JM. Reduction of the lamina cribrosa curvature after trabeculectomy in glaucoma. *Invest Ophthalmol Vis Sci*. 2016;57:5006–5014.

Investigative Ophthalmology & Visual Science